

Time-dependent scattering of a composite particle: A local self-energy approach for internal excitations

Federico Grasselli,^{1,2,*} Andrea Bertoni,^{2,†} and Guido Goldoni^{1,2,‡}

¹*Dipartimento di Scienze Fisiche, Informatiche e Matematiche, Università degli Studi di Modena e Reggio Emilia, Via Campi 213/a, Modena, Italy*

²*S3, Consiglio Nazionale delle Ricerche, Istituto Nanoscienze, Via Campi 213/a, Modena, Italy*

(Received 16 May 2016; published 14 September 2016)

When composite particles—such as small molecules, nuclei, or photogenerated excitons in semiconductors—are scattered by an external potential, energy may be transferred between the c.m. and the internal degrees of freedom. An accurate dynamical modeling of this effect is pivotal in predicting diverse scattering quantities and reaction cross sections, and allows us to rationalize time-resolved energy and localization spectra. Here, we show that time-dependent scattering of a quantum composite particle with an arbitrary, nonperturbative external potential can be obtained by propagating the c.m. degrees of freedom with a properly designed local self-energy potential. The latter embeds the effect of internal virtual transitions and can be obtained by the knowledge of the stationary internal states. The case is made by simulating Wannier-Mott excitons in one- and two-dimensional semiconductor heterostructures. The self-energy approach shows very good agreement with numerically exact Schrödinger propagation for scattering potentials where a mean-field model cannot be applied, at a dramatically reduced computational cost.

DOI: [10.1103/PhysRevB.94.125418](https://doi.org/10.1103/PhysRevB.94.125418)

I. INTRODUCTION

Single-particle scattering is a basic exercise in wave quantum mechanics, but becomes a complex far-reaching problem even for the simplest composite system, a bound pair—say a light diatomic molecule or nuclei [1]. A scattering potential, breaking translational invariance, generally entangles the c.m. and relative degrees of freedom (DOFs) and energy transfer may occur between them [2]. Even when energy conservation does not allow internal excitations, virtual transitions between internal states cannot be neglected. Such mechanisms turn out to be essential in determining scattering coefficients, and should be carefully included for a quantitative evaluation of, e.g., reaction cross sections in heavy-nuclei fusion [1], chemisorption/backscattering ratio in diatomic molecule/surface collisions [3], non-adiabatic electronuclear quantum dynamics [4], lightwave-driven quasiparticle collisions [5], or resonant tunneling of two-particle systems [6].

While in many instances the physics is clear, the problem is how to perform accurate calculations for arbitrary, nonperturbative scattering potentials. A natural and general strategy is to evolve a wave packet with N DOFs according to the time-dependent (TD) Schrödinger equation. Compared to steady-state calculations [7], the TD approach has the advantage that continuum states are naturally taken into account, besides being intuitive and directly applicable to TD potentials [8,9]. Unfortunately, however, the computational load scales exponentially with N . In practice, therefore, drastic simplifications are used, such as reducing the number of DOFs, as in collinear scattering [10], or mean-field (MF) methods are adopted [11].

Here we show that c.m. and relative DOFs can be untangled by using a properly designed self-energy (SE) potential, which embeds the effect of internal virtual transitions. In the proposed approach, a N -DOF propagation is reduced to the TD propagation of the c.m. coordinates alone in an energy-dependent effective potential [12]. The SE, in turn, is obtained from the knowledge of a few internal states, calculated by standard methods for stationary problems. The case is made with a particularly severe test bed, namely indirect Wannier-Mott excitons (IXs), i.e., Coulomb-bound electron-hole pairs, in semiconductor heterostructures. Numerically exact calculations are feasible for the real system in one and two dimensions, and serve as a benchmark for the proposed SE method. At the same time it is an experimentally accessible system, where the scattering potential can be engineered, and predicted space- and time-domain dynamics can be probed by optical means. We investigate common situations where MF methods, based on the adiabatic factorization of the wave function, completely fail to reproduce exact dynamics [13]. The SE method, instead, including in a local potential the virtual transitions to the internal states, provides a TD c.m. wave-packet dynamics which is very close to the results obtained by numerically exact propagation of the full two-body system, at a drastically reduced computational cost.

In Sec. II we describe the physical system under examination, and give the specific parameters used in our simulations for the prototypical case of a Wannier-Mott IX in GaAs-based heterostructures. In Sec. III we describe the numerical method for propagating the composite particle. In Sec. IV we give the general derivation of the SE approach, as well as a description of the MF approximations, whose results are compared to the exact propagation in Secs. VA and VB, for one- and two-dimensional systems, respectively. In Sec. VI we draw concluding remarks and further perspectives of this work. Finally, the Appendix reports details of the derivation of the Green-function local formulation, which gives rise to the *local* SE.

*federico.grasselli@unimore.it

†andrea.bertoni@nano.cnr.it

‡guido.goldoni@unimore.it

II. PHYSICAL SYSTEM

IXs are Coulomb-bound photoexcited electron-hole pairs, with the electron and the hole separated in different layers of a properly engineered semiconductor heterostructure [14,15]. Study of IX scattering dynamics in traps [16], ramps [17], or arbitrary potential landscapes [18] is possible by optical spectroscopy on the sub-ns time scale, as well as the emergence of IX Bose-Einstein condensation [19,20].

Let us consider an electron-hole pair with coordinates and masses $\mathbf{r}_e, \mathbf{r}_h$ and m_e, m_h , respectively, with c.m. and relative coordinates $\mathbf{R} = (m_e \mathbf{r}_e + m_h \mathbf{r}_h)/M$, $\mathbf{r} \equiv \mathbf{r}_e - \mathbf{r}_h$, and total and reduced masses $M = m_e + m_h$ and $m = (m_e^{-1} + m_h^{-1})^{-1}$, respectively. If no external potential is present, the internal IX eigenstates ϕ_n are determined by the relative electron-hole Hamiltonian $-(\hbar^2/2m)\nabla_{\mathbf{r}}^2 + V_{\text{int}}(r)$, with $V_{\text{int}}(r)$ the electron-hole interaction. Including an external potential $V_{\text{ext}} = V_e(\mathbf{r}_e) + V_h(\mathbf{r}_h)$ acting on each particle separately, the total Hamiltonian reads

$$H_{\text{tot}} = -\frac{\hbar^2 \nabla_{\mathbf{R}}^2}{2M} - \frac{\hbar^2 \nabla_{\mathbf{r}}^2}{2m} + V_{\text{int}}(r) + V_{\text{ext}}(\mathbf{R}, \mathbf{r}), \quad (1)$$

where c.m. and relative DOFs are in general coupled.

Note that V_e and V_h are generally different. In semiconductor systems, e.g., they can be generated by a metallic gate, having opposite sign for the two particles. Below we shall perform TD propagation of an IX wave packet under the effect of H_{tot} , comparing numerical exact propagation and the SE approach. In all calculations we assumed typical parameters for GaAs-based materials: electron effective mass $m_e = 0.067m_0$, in-plane heavy-hole effective mass $m_h = 0.111m_0$, and the relative dielectric permittivity $\epsilon_r = 12.9$.

III. EXACT PROPAGATION

Exact TD propagation of the electron-hole wave packet under the effect of H_{tot} can be obtained numerically. In our calculations the wave packet is initialized as $\Psi(\mathbf{R}, \mathbf{r}; t=0) = \chi_G(\mathbf{R})\phi_0(\mathbf{r})$, where $\chi_G(\mathbf{R}) \propto \exp(i\mathbf{K}_0 \cdot \mathbf{R}) \exp(-|\mathbf{R} - \mathbf{R}_0|^2/4\sigma^2)$ is a Gaussian envelope centered at \mathbf{R}_0 of width σ , initially vanishing in the scattering region, with most probable c.m. initial kinetic energy $E_{\text{c.m.}} = \hbar^2 K_0^2/2M$. The repeated application of the unitary evolution operator $\mathcal{U}(t + \Delta t, t)$ between times t and $t + \Delta t$, is performed with the Fourier split-step (FSS) method [13,21],

$$\Psi(\mathbf{R}, \mathbf{r}; t + \Delta t) = \mathcal{U}(t + \Delta t, t)\Psi(\mathbf{R}, \mathbf{r}; t). \quad (2)$$

Note that, even though the initial wave packet is factorized, no assumption is made during propagation. Later we will analyze the results of the TD evolution in terms of the marginal probability $\rho_{\text{c.m.}}(\mathbf{R}; t) \equiv \int d\mathbf{r} |\Psi(\mathbf{R}, \mathbf{r}; t)|^2$, which can be understood as the c.m. probability density.

IV. SELF-ENERGY APPROACH

A general wave packet at time t can be written as

$$\Psi(\mathbf{R}, \mathbf{r}; t) = \sum_n \chi_n(\mathbf{R}; t)\phi_n(\mathbf{r}), \quad (3)$$

where the c.m. envelopes χ_n are coefficients in the *exact* expansion over the complete set of internal eigenstates,

$\phi_n(\mathbf{r})$ [the sum in Eq. (3) can be possibly extended to the continuum states]. Using (3), we recast the TD Schrödinger equation $(H_{\text{tot}} - i\hbar\partial_t)\Psi(\mathbf{R}, \mathbf{r}; t) = 0$ in the *coupled channel equations* [2] for the χ_n ,

$$\sum_n (\mathcal{H}_{mn}(\mathbf{R}) - i\hbar\partial_t \delta_{mn})\chi_n = 0, \quad m = 0, 1, 2, \dots, \quad (4)$$

where

$$\mathcal{H}_{mn} = \left[-\frac{\hbar^2 \nabla_{\mathbf{R}}^2}{2M} + \epsilon_m \right] \delta_{mn} + W_{mn}(\mathbf{R}), \quad (5)$$

$$W_{mn}(\mathbf{R}) = \int d\mathbf{r} \phi_m^*(\mathbf{r}) V_{\text{ext}}(\mathbf{R}, \mathbf{r}) \phi_n(\mathbf{r}). \quad (6)$$

If Eq. (3) is not truncated, Eqs. (4) give the exact propagation, just like Eq. (2).

After expressing $\chi_n(\mathbf{R}; t)$ in terms of the energy Fourier components $\tilde{\chi}_n(\mathbf{R}; E)$, and assuming the variance on $E_{\text{c.m.}}$ is small compared to the absolute value of the total (most probable) energy $E = E_{\text{c.m.}} + \epsilon_0$, we obtain an equation for $\tilde{\chi}_0$, by treating couplings to higher envelopes, $\tilde{\chi}_{n \neq 0}$, in second-order perturbation theory following Löwdin [22],

$$\mathcal{H}_{00}\tilde{\chi}_0 + \int d\mathbf{R}' \Sigma_0(\mathbf{R}, \mathbf{R}'; E)\tilde{\chi}_0(\mathbf{R}'; E) = E\tilde{\chi}_0. \quad (7)$$

This amounts to neglecting couplings *between* higher internal states, i.e., $\mathcal{H}_{mn} \equiv 0$ if $n \neq m$ and $n, m > 0$. In our simulations, with wave-packet spatial dispersion $\sigma \sim 150$ nm, the relative variance on $E_{\text{c.m.}}$ is ~ 0.02 meV $\ll E_{\text{c.m.}} \sim 0.2$ meV $\ll |E| \sim$ few meV. The term \mathcal{H}_{00} in Eq. (7) represents the Hamiltonian of an electron-hole pair with the c.m. which moves in the average potential $W_{00}(\mathbf{R}) = \int d\mathbf{r} |\phi_0(\mathbf{r})|^2 V_{\text{ext}}(\mathbf{R}, \mathbf{r})$. This corresponds to a factorized wave function $\Psi(\mathbf{R}, \mathbf{r}; t) = \chi_0(\mathbf{R}; t)\phi_0(\mathbf{r})$, i.e., with the IX frozen in its relative-motion ground state. Note that, in general, a MF approximation assumes an *ansatz* $\Psi^{\text{MF}}(\mathbf{R}, \mathbf{r}; t) = \chi^{\text{MF}}(\mathbf{R}; t)\phi^{\text{MF}}(\mathbf{r}; t)$ which, inserted in the Schrödinger equation, leads to two coupled TD equations for $\chi^{\text{MF}}(\mathbf{R}; t)$ and $\phi^{\text{MF}}(\mathbf{r}; t)$, which should be evolved iteratively [11]. Therefore, \mathcal{H}_{00} can be understood as a *rigid*-MF (RMF) approximation, with $\phi^{\text{MF}}(\mathbf{r}; t) = \phi_0(\mathbf{r})$. In semiconductor physics this is known as the *rigid exciton model* [23].

In Eq. (7) $\Sigma_0(\mathbf{R}, \mathbf{R}'; E)$ is a c.m. *self-interaction* which arises from virtual transitions between the ground and the excited internal states, induced by the c.m. propagation under the effect of W_{00} ,

$$\Sigma_0(\mathbf{R}, \mathbf{R}'; E) = \sum_{m \neq 0} W_{0m}(\mathbf{R}) G_m(\mathbf{R}, \mathbf{R}'; E) W_{m0}(\mathbf{R}'), \quad (8)$$

where $G_m(\mathbf{R}, \mathbf{R}'; E) = (\mathbf{R} | (E - \hat{\mathcal{H}}_{mm})^{-1} | \mathbf{R}')$ is the Green function for the m th c.m. problem.

We now specialize to one dimension and we approximate G_m with the one-dimensional (1D) free-particle Green function $G_m^{(f)}$,

$$G_m^{(f)}(R, R'; E) = -\frac{M}{\hbar^2 \kappa_m} \exp(-\kappa_m |R - R'|), \quad (9)$$

where $\kappa_m \equiv \sqrt{2M|E - \epsilon_m|/\hbar}$. This represents an evanescent wave, since we assume that the system is initialized into the internal ground state with $E - \epsilon_m < 0, \forall m > 0$, implying that

$G_m^{(f)}$, hence $\Sigma_0^{(f)}$, are real functions. For explicit calculations, we obtain a *local* approximation under the assumption that κ_m is so large that $G_m^{(f)} \approx 0$ for paths (virtually) traveled by the c.m. $|R - R'| \gtrsim \kappa_m^{-1}$. Then (see Appendix)

$$G_m^{(f)}(R, R'; E) \sim -\frac{2M}{\hbar^2 \kappa_m^2} \delta(R - R') = \frac{\delta(R - R')}{E - \epsilon_m}, \quad (10)$$

which leads to a *local SE*

$$\Sigma_0^{(f)}(R, R'; E) = \delta(R - R') \sum_{m \neq 0}^{N_c} \frac{|W_{0m}(R)|^2}{E - \epsilon_m}. \quad (11)$$

The sum in Eq. (11) should be extended to a sufficiently large number N_c of internal IX eigenstates for convergent results. Typically N_c is in the order of a few units (see Supplemental Material [24]).

In the limit of large wave vector it is appropriate to assume a semiclassical approximation $G_m^{(scl)} \propto \exp[iS_m^{(scl)}(R, R'; E)/\hbar]$, where $S_m^{(scl)}(R, R'; E) = \int_{\gamma_{R,R'}} \hbar K_m(R'') dR''$ is the classical action, $\gamma_{R,R'}$ being the *classical* path from R to R' . For large imaginary $K_m = i\kappa_m$, the latter can be expanded at the first order in $|R - R'|$ [25], leading to semiclassical expressions for the *localized* Green function and SE which are still of the form (11) but with the substitution

$$E - \epsilon_m \longrightarrow E - \epsilon_m - W_{mm}(R). \quad (12)$$

We indicate the right-hand side of Eq. (11), with substitution (12), as $\Sigma_0^{(scl)}$.

The previous SE approach can be generalized to two dimensions. The free-particle Green function now reads

$$G_m^{(f)}(\mathbf{R}, \mathbf{R}'; E) = -\frac{M}{\pi \hbar^2} K_0(\kappa_m |\mathbf{R} - \mathbf{R}'|/\hbar), \quad (13)$$

where K_0 is the modified Bessel function of the second kind. $G_m^{(f)}$ can be cast in a local form, analogous to Eq. (10), $G_m^{(f)}(\mathbf{R}, \mathbf{R}'; E) \approx \delta(\mathbf{R} - \mathbf{R}')/(E - \epsilon_m)$. Again, the denominator becomes $E - \epsilon_m - W_{mm}(\mathbf{R})$ if a semiclassical local correction is included in the Supplemental Material [24]. The related expression for the SE, $\Sigma_0^{(scl)}$, is straightforward.

V. RESULTS

A. One-dimensional systems

We now consider a 1D IX, with c.m. and relative coordinates R, r . The two particles are confined, say, to two quantum wires separated by a distance d , and move along the wires across a square well potential acting on the electron, of depth $V_{e,0}$ and width L , while $V_h = 0$ [see inset in Fig. 1(a)]. The electron-hole Coulomb interaction is $V_{\text{int}}(r) = -e^2/(4\pi\epsilon_0\epsilon_r\sqrt{r^2 + d^2})$, with $\epsilon_0\epsilon_r$ the dielectric permittivity.

We perform exact TD propagation with Eq. (2) for this $N = 2$ problem. To analyze the scattering, we compute the transmission coefficient as $T = \int_{\mathbf{T}} \rho_{c.m.}(R; \bar{t}) dR$ vs the well depth $V_{e,0}$. The integration is carried out over the half space \mathbf{T} [see inset in Fig. 1(a)] at a sufficiently large time \bar{t} for the scattering to be completed. As shown by the solid black line in Fig. 1(a), T displays two strong resonances at $V_{e,0} \simeq -1.4$ and -2.6 meV. Although this is qualitatively expected also in a single-particle picture, estimating the resonance positions

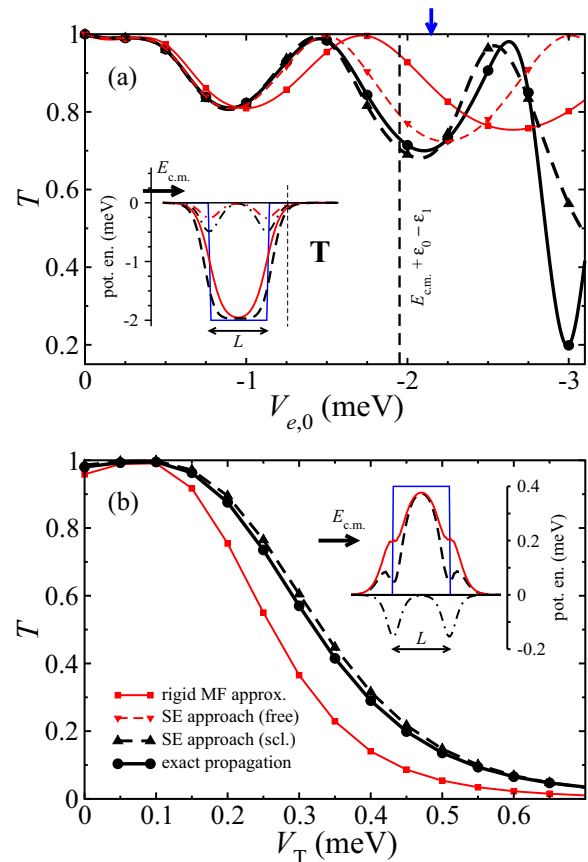


FIG. 1. Calculated transmission T through (a) an electron potential well vs depth $V_{e,0}$, and (b) a hole well and an electron barrier vs the total strength $V_T \equiv V_{e,0} + V_{h,0} \geq 0$. Here, $V_{h,0} = -0.6$ meV, while $V_{e,0}$ is increased from $+0.6$ meV. In (a) a cubic spline is drawn between calculated points; the vertical dashed line indicates the lowest energy for internal excitation, $V_{e,0} = E_{c.m.} + \epsilon_0 - \epsilon_1$, with $\epsilon_0 = -3.86$ meV, $\epsilon_1 = -1.71$ meV. Insets: scattering potentials and SE corrections for (a) $V_{e,0} = -2.0$ meV, and (b) $V_T = +0.4$ meV. Blue line: pointlike-particle potential; red line: RMF potential $W_{00}(R)$; black dashed line: SE-corrected RMF potential $W_{00}(R) + \Sigma_0^{(scl)}(R)$; red dash-dotted line: $\Sigma_0^{(f)}(R)$; black dash-dotted line: $\Sigma_0^{(scl)}(R)$. Here, $N_c = 5$. The transmission region \mathbf{T} is defined from $|W_{00}(R)| < 5\%|V_{e,0}|$. All calculations are performed with $E_{c.m.} = 0.2$ meV, $L = 60$ nm, $d = 20$ nm, $\sigma = 150$ nm. Short animations are presented in the Supplemental Material [24].

for a pointlike exciton with mass M gives wrong resonant energy positions -2.15 meV [see arrow on the top of Fig. 1(a)] and -5.08 meV (i.e., larger, in absolute value, than the IX dissociation energy in the Supplemental Material [24]).

Figure 1(a) shows the transmission T calculated using the SE approach, i.e., propagating $\chi_0(R; t)$ under the total c.m. potential $W_{00} + \Sigma_0^{(scl)}$ (shown by the dashed black line in the inset). This shows a very good agreement with exact calculations up to and beyond the first internal excitation energy (vertical dashed line), accurately reproducing, in particular, both resonance positions. We emphasize that this agreement is obtained by propagating only the c.m. DOF.

To understand the specific role on the c.m. dynamics of internal virtual transitions, in Fig. 1(a) inset we show $\Sigma_0^{(scl)}$

(dash-dotted black line) and the RMF potential W_{00} (solid red line). W_{00} is a smooth potential obtained by averaging the square well potential V_{ext} with $|\phi_0|^2$. The SE $\Sigma_0^{(scl)}$ consists of a weakly attractive term located at the well edges and downshifts the resonances. For comparison, we show in Fig. 1(a) T obtained propagating the c.m. without the substitution (12) (dashed red line), i.e., using $\Sigma_0^{(f)}$ (red dash-dotted line in the inset): it is substantially weaker than $\Sigma_0^{(scl)}$. Overall, the agreement is still good and extends almost to the first internal excitation threshold, but worsens beyond this point. Thus, in the rest of the paper Eq. (12) is used. We also stress that in the SE approach, as well as in the RMF approximation, $\rho_{\text{c.m.}} = |\chi_0(R)|^2$.

We also show for completeness the c.m. transmission in the RMF model, i.e., using only the potential W_{00} (red solid line). Neglecting electron-hole correlations by construction, this is in general unable to reproduce the transmission, except for very low energy. In particular, resonance positions are not reproduced, although somewhat downshifted with respect to the point-particle calculation. This emphasizes the prominent role of internal virtual transitions.

Many physical phenomena are concerned with quantum tunneling of composite particles (see [26–28] and references therein). Therefore, we next investigate tunneling through an overall repulsive barrier composed of an attractive well of depth $V_{h,0} < 0$ for the hole and a repulsive barrier of height $V_{e,0} \geq -V_{h,0}$ for the electron, both of length L . In Fig. 1(b) we show T vs the total potential-energy strength, $V_T = V_{e,0} + V_{h,0}$. As expected, T decreases from ~ 1 , starting from $V_T \approx E_{\text{c.m.}} = 0.2$ meV, to 0, which is reached at $V_T \approx 3E_{\text{c.m.}}$. Remarkably, SE calculations are in almost perfect agreement with exact propagation in the whole range of scattering potential strength. Results with $\Sigma_0^{(f)}$ and $\Sigma_0^{(scl)}$ almost coincide. Figure 1(b) inset shows that, similar to the previous case, $\Sigma_0^{(scl)}$ consists of a negative contribution located at the edges, hence favoring transmission. Indeed, if the SE is neglected, tunneling is severely underestimated, by as much as 50% at $V_T \sim 0.3$ meV.

We emphasize that the good agreement between the SE approach and exact propagation holds at any time *during* the scattering process, as shown in the Supplemental Material [24].

B. Two-dimensional systems

We next consider systems where the electron and the hole are confined in separated 2D layers. An initial wave packet is scattered by a square-shaped potential with side D , composed of a square well $V_{e,0}$ for the electron and a barrier $V_{h,0}$ for the hole, which is overall repulsive, i.e., $V_{h,0} + V_{e,0} > 0$. A more realistic device-based model is adopted here for the electron-hole interaction, from which the internal ϕ_n are calculated. See [13] and [24] for details.

Exact calculations, now a $N = 4$ problem, have been performed using Eq. (2), exploiting massively parallel architectures [13]. Note that sufficiently accurate propagations are quite demanding, typical runs (tens of ps) requiring 2^{32} grid points and ≈ 1000 CPU hours on a high-performance computing infrastructure. A snapshot of the marginal probability $\rho_{\text{c.m.}}(\mathbf{R}; t)$ is shown in Fig. 2(d). Approximately half of the wave packet is reflected in one bunch, while the transmitted part separates into a diffraction pattern. In addition, part of the wave packet remains localized for a long time at the edges of the external potential.

Calculations for the c.m. propagation with the SE method [Fig. 2(c)] shows very good agreement with exact calculations. In particular, the diffraction pattern is fully reproduced, with minor differences in peak intensities. Also the wave-packet localization at the boundaries of the scattering potential is partially reproduced. Note that these calculations, involving only the two c.m. DOFs, could be performed on a personal workstation in minutes. We also show in Fig. 2(b) the result in the RMF approximation. Here, the c.m. wave packet is in striking contrast with the exact calculation: The transmitted wave packet is divided in two large lobes, and no diffraction pattern forms, nor does any localization at the potential edges take place.

This striking difference can be understood from Fig. 2(a) where we show $\Sigma_0^{(scl)}$ along a section of the scattering potential. The SE consists of a negative term along the edge of the potential, where the IX wave packet partially localizes during the scattering event. From a semiclassical point of view, this corresponds to the binding of the electron and the hole on opposite sides of the square potential, due to the reciprocal Coulomb interaction. Clearly this cannot be captured by the RMF calculation, but it is correctly described by the SE calculation.

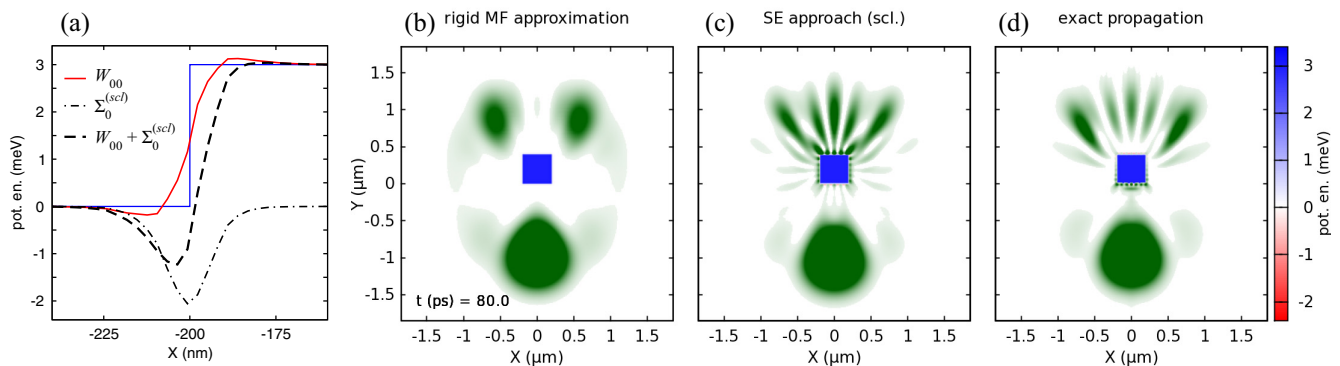


FIG. 2. IX scattering against an overall square repulsive potential with $D = 400$ nm, $V_{h,0} = +6.0$ meV, $V_{e,0} = -3.0$ meV. (a) Effective potential-energy profiles calculated at $Y = D/2$. Blue: pointlike-particle potential; red: W_{00} ; black dashed line: $W_{00} + \Sigma_0^{(scl)}$; black dash-dotted line: $\Sigma_0^{(scl)}$. Here, $N_c = 7$. (b)–(d) Snapshots of the c.m. marginal probability density $\rho_{\text{c.m.}}(\mathbf{R}; t)$ at $t = 80$ ps in the RMF model, the SE approach, and in the exact propagation, as indicated. A short animation is presented in the Supplemental Material [24].

The diffraction pattern is due to the lateral localization of the IX wave packet in the SE: the number of nodes of the localized state determines the number N_l of diffraction lobes. It can be estimated that $N_l \leq \sqrt{2M(E_{\text{c.m.}} + \sup|W_{00} + \Sigma_0|)/(\hbar\pi D)}$ (a case with a larger $E_{\text{c.m.}}$ is provided in the Supplemental Material [24]).

VI. CONCLUSIONS

Overall, the present SE approach exposes the prominent role of virtual transitions in low-energy scattering and offers a computational method to reduce the propagation of a composite particle in a scattering potential to the propagation of the c.m. DOFs alone with an energy-dependent term added to the RMF potential. For realistic 1D and 2D cases examined here, quantitative agreement with exact calculations is demonstrated. A MF calculation, neglecting internal correlations, is intrinsically unable to capture the correct physics in the above cases. This has been shown here with RMF calculations. However, we have checked that a TD Hartree approach [11,13], i.e., a MF approach with a TD self-consistently calculated relative wave function $\phi^{\text{MF}}(\mathbf{r};t)$, gives results which are equivalent to the RMF calculations.

Although validated here for the 1D and 2D cases due to computational limitations of the exact propagation, the SE method can be formally generalized to 3D systems, as we discuss in Appendix A. Likely, the larger the dimensionality, the greater the number of internal eigenstates of the pair to be included to achieve convergence of the SE, due to level degeneracy.

We emphasize that the proposed SE method, thanks to the *local* formulation of the SE, allows for a dramatic reduction in computational time. In turn, the SE is calculated from the knowledge of a few unperturbed internal states. Therefore, the proposed SE approach can be extended to more than two particles, provided an adequate number of internal excited states is known, as well as to TD external potentials. We also note that it can be extended to larger scattering potentials and/or kinetic energies, comparable to the internal gaps. This can be obtained by folding the coupled channel equations (4) on a sufficiently large number of coupled differential equations for the χ_n . We checked that for IXs this does not improve the agreement with exact calculations at larger energies, e.g., in Fig. 1(a). We ascribe this to the specific interparticle interaction (here a Coulomb potential) whose excited states become rapidly dense in energy. We speculate that the situation might be more favorable, for example, for nuclear potentials or molecular vibronic states. In these systems hard wall or nearly harmonic potentials result in more regular level spacing.

ACKNOWLEDGMENTS

We acknowledge a CINECA award under ISCR C project IsC33- "FUQUDEX." We acknowledge useful discussions with M. Rontani and G. Gil.

APPENDIX : LOCAL APPROXIMATION FOR THE GREEN FUNCTION

In the *local approximation* the transition to a higher level and its decay again into the internal ground state are considered

to happen *at the same point* \mathbf{R} in the center-of-mass (c.m.) space.

The *free particle* Green function for the c.m. m th state reads [29] as follows: (i) in one dimension,

$$G_m^{(f)}(R, R'; E) = \frac{M}{i\hbar\sqrt{2M(E - \epsilon_m)}} \times \exp\left[\frac{i}{\hbar}\sqrt{2M(E - \epsilon_m)}|R - R'|\right]; \quad (\text{A1})$$

(ii) in two dimensions,

$$G_m^{(f)}(\mathbf{R}, \mathbf{R}'; E) = -\frac{M}{\pi\hbar^2} \times K_0[\sqrt{-2M(E - \epsilon_m + i0^+)}|\mathbf{R} - \mathbf{R}'|/\hbar], \quad (\text{A2})$$

where $K_{\nu=0}$ is the modified Bessel function of the second kind, and 0^+ is an arbitrarily small positive constant; (iii) in three dimensions,

$$G_m^{(f)}(\mathbf{R}, \mathbf{R}'; E) = -\frac{1}{2\pi\hbar^2} \frac{M}{|\mathbf{R} - \mathbf{R}'|} \times \exp\left[\frac{i}{\hbar}\sqrt{2M(E - \epsilon_m)}|\mathbf{R} - \mathbf{R}'|\right]. \quad (\text{A3})$$

The extension to negative c.m. (kinetic) energies ($E - \epsilon_m < 0$), for the m th level, is straightforward. The latter implies, incidentally, that the exponent of the exponential becomes negative, rather than an imaginary number: in such a case, instead of propagating, the c.m. wave function corresponding to an excited internal state decreases exponentially, the propagator being an evanescent function.

If the modulus of the wave vector, $\kappa_m \equiv \sqrt{2M|E - \epsilon_m|}/\hbar$ is so large that for (either virtual or real) paths traveled by the c.m. the following condition holds:

$$|\mathbf{R} - \mathbf{R}'| \gtrsim \kappa_m^{-1}, \quad (\text{A4})$$

the Green function $G_m^{(f)}$ behaves, under integration, as a Dirac δ function,

$$G_m^{(f)}(\mathbf{R}, \mathbf{R}'; E) \sim f(\mathbf{R}; E)\delta(\mathbf{R} - \mathbf{R}'), \quad (\text{A5})$$

where $f(\mathbf{R}; E)$ is a possibly c.m.-position-dependent (complex) function to be obtained by δ function normalization.

Below we give the detailed and explicit calculations for the 1D and the 2D cases, and for imaginary wave vectors (real, decreasing exponential factors), since these are the cases we have considered for the numerical simulations in the main paper. The calculation with real wave vectors can be obtained easily within the Fourier representation of the δ function.

In one dimension,

$$\begin{aligned} & \int_{-\infty}^{+\infty} G_m^{(f)}(R, R'; E) dR' \\ &= \int_{-\infty}^{+\infty} -\frac{M}{\hbar^2\kappa_m} \exp(-\kappa_m|R - R'|) dR' \\ &= -\frac{2M}{\hbar^2\kappa_m} \int_0^{+\infty} \exp(-\kappa_m R'') dR'' = -\frac{2M}{\hbar^2\kappa_m^2}. \end{aligned} \quad (\text{A6})$$

Hence the localized form for the Green function becomes

$$G_m^{(f)}(\mathbf{R}, \mathbf{R}'; E) \sim -\frac{2M}{\hbar^2 \kappa_m^2} \delta(\mathbf{R} - \mathbf{R}') = \frac{\delta(\mathbf{R} - \mathbf{R}')}{E - \epsilon_m}. \quad (\text{A7})$$

Equivalently, in two dimensions,

$$\begin{aligned} & \iint d^2 \mathbf{R}' G_m^{(f)}(\mathbf{R}, \mathbf{R}'; E) \\ &= -\frac{M}{\pi \hbar^2} 2\pi \int_0^\infty d|\mathbf{R}''| |\mathbf{R}''| K_0(\kappa_m |\mathbf{R}''|) = -\frac{2M}{\hbar^2 \kappa_m^2}, \end{aligned} \quad (\text{A8})$$

where we used the integral property of Bessel's functions

$$\int_0^\infty dz z K_0(z) = 1. \quad (\text{A9})$$

Therefore, in the limit of large modulus of the wave vector, we obtain

$$G_m^{(f)}(\mathbf{R}, \mathbf{R}'; E) \sim -\frac{2M}{\hbar^2 \kappa_m^2} \delta(|\mathbf{R} - \mathbf{R}'|) = \frac{\delta(|\mathbf{R} - \mathbf{R}'|)}{E - \epsilon_m}. \quad (\text{A10})$$

It is important to note that the results in terms of the energy (right sides of the above equations) hold not only for imaginary wave vectors, but also for real ones, as one can immediately verify by means of the Fourier integral representation of Dirac's δ . In such a case, the denominator $E - \epsilon_m$ shall be positive. Therefore, the final results are still valid for real propagation, even though the whole problem will no longer be sufficiently described by the SE approach for the propagation of the c.m. wave function corresponding to the ground state, since also the excitation to higher levels would be allowed due to energy conservation.

We can further develop the model by adopting a semiclassical formulation for the Green function. Its general formulation in d dimensions is given by [25]

$$\begin{aligned} G_m^{(sc)}(\mathbf{R}, \mathbf{R}'; E) &= \frac{1}{i\hbar} \frac{1}{(2\pi i\hbar)^{(d+1)/2}} \sum_{\text{class. paths}} |\mathcal{D}_S|^{1/2} \\ &\times \exp \left[\frac{i S_m^{(cl)}(\mathbf{R}, \mathbf{R}'; E)}{\hbar} + \text{phases} \right], \end{aligned} \quad (\text{A11})$$

where

$$\mathcal{D}_S \equiv (-1)^{d+1} \begin{vmatrix} \frac{\partial^2 S_m^{(cl)}}{\partial \mathbf{R}' \partial \mathbf{R}} & \frac{\partial^2 S_m^{(cl)}}{\partial \mathbf{R}' \partial E} \\ \frac{\partial^2 S_m^{(cl)}}{\partial E \partial \mathbf{R}} & \frac{\partial^2 S_m^{(cl)}}{\partial E^2} \end{vmatrix}, \quad (\text{A12})$$

and

$$S_m^{(cl)}(\mathbf{R}, \mathbf{R}'; E) \equiv \int_{\gamma_{\mathbf{R}' \rightarrow \mathbf{R}}} \hbar \mathbf{K}_m \cdot d\mathbf{R}'' \quad (\text{A13})$$

is the classical action of the c.m. m th problem evaluated along the classical trajectory $\gamma_{\mathbf{R}' \rightarrow \mathbf{R}}$ going from the point \mathbf{R}' to the point \mathbf{R} at the energy E [30], $\mathbf{K}_m(\mathbf{R}'') \equiv \nabla_{\mathbf{R}''} S_m^{(cl)}(\mathbf{R}'', \mathbf{R}'; E)$, and the possible additional phases account for the number of conjugate times along the classical trajectory [25].

In general, the computation of $G_m^{(sc)}(\mathbf{R}, \mathbf{R}'; E)$ is strictly dependent on the specific dimensionality and potential landscape, since it requires to calculate the classical action functional $S_m^{(cl)}(\mathbf{R}, \mathbf{R}'; E)$, as well as its derivative, which implies in general to solve the Euler-Lagrange equations of the system, also in order to find the classical trajectory $\gamma_{\mathbf{R}' \rightarrow \mathbf{R}}$.

A great simplification is given if we consider short paths and expand the classical action in powers of $|\mathbf{R} - \mathbf{R}'|$. If we truncate at the first order, the action becomes

$$\begin{aligned} S_m^{(cl)}(\mathbf{R}, \mathbf{R}'; E) &\approx |\hbar \mathbf{K}_m(\mathbf{R})| |\mathbf{R} - \mathbf{R}'| \\ &= \sqrt{2M(E - \epsilon_m - W_{mm}(\mathbf{R}))} |\mathbf{R} - \mathbf{R}'|, \end{aligned} \quad (\text{A14})$$

where $W_{mm}(\mathbf{R})$ is defined in Eq. (6). This expansion is justified in view of a local formulation for the Green functions (now with further semiclassical contribution). This leads to expressions for the Green functions which are formally coincident with the free particle ones, once we replace $E - \epsilon_m$ with $E - \epsilon_m - W_{mm}(\mathbf{R})$.

In order to find the correct normalization for the δ , we consider the fact that, under our locality assumptions, the potential $W_{mm}(\mathbf{R})$ can be considered as a constant while the integration as in Eqs. (A6) and (A8) is performed.

Finally we have

$$G_m^{(sc)}(\mathbf{R}, \mathbf{R}'; E) = \frac{\delta(|\mathbf{R} - \mathbf{R}'|)}{E - \epsilon_m - W_{mm}(\mathbf{R})}, \quad (\text{A15})$$

where the δ function is to be intended in the correct dimensionality. Here, the denominator too is dependent on the specific position, being the *local* c.m. kinetic energy of the m th problem. In order to adopt Eq. (A15), one must keep in mind that the working assumption is that $\kappa_m(\mathbf{R})$ must have large values. If this was not the case, the denominator in Eq. (A15), and thus the one in the self-energy, would vanish, leading to divergences [which can be associated to the formation of a bound state, but which dramatically affect the propagation, since Eq. (A15) would be no longer a good expression]. At a given m , this happens for all the c.m. points \mathbf{R} where $E - \epsilon_m - W_{mm}(\mathbf{R}) = 0$, i.e., wherever the c.m. ground level energy, $E_{c.m.,0} \equiv E - \epsilon_0$, is $E_{c.m.,0} = |\epsilon_0 - \epsilon_m| + W_{mm}(\mathbf{R})$.

Note that, since Σ_0 contains the sum for each m of terms like $[E - \epsilon_m - W_{mm}(\mathbf{R})]^{-1}$, it suffices that this diverges in a c.m. region, for *just one* specific m , for the whole Σ_0 to exhibit divergences in the same region. We denote the c.m. kinetic energy for $m = 0$, $E_{c.m.,0}$, simply by $E_{c.m.}$.

[1] A. B. Balantekin and N. Takigawa, Quantum tunneling in nuclear fusion, *Rev. Mod. Phys.* **70**, 77 (1998).

[2] N. Ahsan and A. Volya, Quantum tunneling and scattering of a composite object reexamined, *Phys. Rev. C* **82**, 064607 (2010).

- [3] G.-J. Kroes and C. Díaz, Quantum and classical dynamics of reactive scattering of H_2 from metal surfaces, *Chem. Soc. Rev.* **45**, 3658 (2016).
- [4] J. Albert, D. Kaiser, and V. Engel, Communication: Adiabatic and non-adiabatic electron-nuclear motion: Quantum and classical dynamics, *J. Chem. Phys.* **144**, 171103 (2016).
- [5] F. Langer, M. Hohenleutner, C. P. Schmid, C. Poellmann, P. Nagler, T. Korn, C. Schüller, M. S. Sherwin, U. Huttner, J. T. Steiner, S. W. Koch, M. Kira, and R. Huber, Lightwave-driven quasiparticle collisions on a subcycle timescale, *Nature (London)* **533**, 225 (2016).
- [6] N. Saito and Y. Kayanuma, Resonant tunnelling of a composite particle through a single potential barrier, *J. Phys.: Condens. Matter* **6**, 3759 (1994).
- [7] A. Bertoni and G. Goldoni, Phase lapses in scattering through multielectron quantum dots: Mean-field and few-particle regimes, *Phys. Rev. B* **75**, 235318 (2007).
- [8] B. Gaury, J. Weston, M. Santin, M. Houzet, C. Groth, and X. Waintal, Numerical simulations of time-resolved quantum electronics, *Phys. Rep.* **534**, 1 (2014).
- [9] F. Buscemi, P. Bordone, and A. Bertoni, Quantum teleportation of electrons in quantum wires with surface acoustic waves, *Phys. Rev. B* **81**, 045312 (2010).
- [10] A. V. Lugovskoy and I. Bray, Pseudostate description of diatomic-molecule scattering from a hard-wall potential, *Phys. Rev. A* **87**, 012904 (2013).
- [11] M. H. Beck, A. Jäckle, G. A. Worth, and H. D. Meyer, The multiconfiguration time-dependent Hartree (MCTDH) method: a highly efficient algorithm for propagating wavepackets, *Phys. Rep.* **324**, 1 (2000).
- [12] Yu. A. Kuperin, and Yu. B. Melnikov, Two-body resonance scattering and annihilation of composite charged particles, *J. Math. Phys.* **33**, 2795 (1992).
- [13] F. Grasselli, A. Bertoni, and G. Goldoni, Exact two-body quantum dynamics of an electron-hole pair in semiconductor coupled quantum wells: a time dependent approach, *Phys. Rev. B* **93**, 195310 (2016).
- [14] L. V. Butov, C. W. Lai, A. L. Ivanov, A. C. Gossard, and D. S. Chemla, Towards bose-einstein condensation of excitons in potential traps, *Nature (London)* **417**, 47 (2002).
- [15] K. Sivalertporn, L. Mouchliadis, A. L. Ivanov, R. Philp, and E. A. Muljarov, Direct and indirect excitons in semiconductor coupled quantum wells in an applied electric field, *Phys. Rev. B* **85**, 045207 (2012).
- [16] G. J. Schinner, J. Repp, E. Schubert, A. K. Rai, D. Reuter, A. D. Wieck, A. O. Govorov, A. W. Holleitner, and J. P. Kotthaus, Confinement and Interaction of Single Indirect Excitons in a Voltage-Controlled Trap Formed Inside Double InGaAs Quantum wells, *Phys. Rev. Lett.* **110**, 127403 (2013).
- [17] A. Gärtner, A. W. Holleitner, J. P. Kotthaus, and D. Schuh, Drift mobility of long-living excitons in coupled gaas quantum wells, *Appl. Phys. Lett.* **89**, 052108 (2006).
- [18] P. Andreakou, S. V. Poltavtsev, J. R. Leonard, E. V. Calman, M. Remeika, Y. Y. Kuznetsova, L. V. Butov, J. Wilkes, M. Hanson, and A. C. Gossard, Optically controlled excitonic transistor, *Appl. Phys. Lett.* **104**, 091101 (2014).
- [19] A. A. High, J. R. Leonard, A. T. Hammack, M. M. Fogler, L. V. Butov, A. V. Kavokin, K. L. Campman, and A. C. Gossard, Spontaneous coherence in a cold exciton gas, *Nature (London)* **483**, 584 (2012).
- [20] M. Alloing, M. Beian, M. Lewenstein, D. Fuster, Y. González, L. González, R. Combescot, M. Combescot, and F. Dubin, Evidence for a Bose-Einstein condensate of excitons, *Europhys. Lett.* **107**, 10012 (2014).
- [21] F. Grasselli, A. Bertoni, and G. Goldoni, Space- and time-dependent quantum dynamics of spatially indirect excitons in semiconductor heterostructures, *J. Chem. Phys.* **142**, 034701 (2015).
- [22] P.-O. Löwdin, A note on the quantum mechanical perturbation theory, *J. Chem. Phys.* **19**, 1396 (1951).
- [23] R. Zimmermann, F. Große, and E. Runge, Excitons in semiconductor nanostructures with disorder, *Pure Appl. Chem.* **69**, 1179 (1997).
- [24] See Supplemental Material at <http://link.aps.org/supplemental/10.1103/PhysRevB.94.125418> for numerical details and parameters, further simulations and convergence tests, and short animations of selected cases.
- [25] M. C. Gutzwiller, Phase-integral approximation in momentum space and the bound states of an atom, *J. Math. Phys.* **8**, 1979 (1967).
- [26] C. A. Bertulani, V. V. Flambaum, and V. G. Zelevinsky, Tunneling of a composite particle: effects of intrinsic structure, *J. Phys. G: Nucl. Part. Phys.* **34**, 2289 (2007).
- [27] J. J. Kavka, D. Kerbrat, and M. R. A. Shegelski, Quantum tunneling and reflection of a molecule with a single bound state, *Phys. Rev. A* **81**, 022708 (2010).
- [28] M. Rontani, Pair tunneling of two atoms out of a trap, *Phys. Rev. A* **88**, 043633 (2013).
- [29] M. C. Gutzwiller, Energy spectrum according to classical mechanics, *J. Math. Phys.* **11**, 1791 (1970).
- [30] Expressing it in terms either of the total energy or of the c.m. m th problem energy is equivalent, since $E_{c.m.,m} = E - \epsilon_m$.